Electronic Supplementary Information

Interlayer sliding induced antiferroelectricity-ferroelectricity-antiferroelectricity transition in bilayer *δ*-SiX (X = S/Se)

Zihan Qu [1], Xiaoteng Wang [1], Jishun Zhang [1], Shuo Jiang [1], Zuyu Xu [1], Fei Yang [1], Zuheng Wu [1]*, Yuehua Dai [1]*, and Yunlai Zhu [1]*

[a] School of Integrated Circuits, Anhui University, Hefei, Anhui, 230601, China.

Corresponding Authors

*E-mail: wuzuheng@ahu.edu.cn (Z.-H. Wu), daiyuehua2013@163.com (Y.-H. Dai), zhuyunlai@ahu.edu.cn (Y.-L. Zhu)

S1. Interpretation of AA-AB, AA-AC, AA-AD slip path in top views.

In order to simplify the process of configuration sliding, we only select a part of the AA configuration (highlighted region 1) as a schematic. To transition to AB stacking, we shift the upper SiS layer of the AA configuration by *a*/2 along the *x*-axis, as illustrated in **Fig. S1(a)**. Similarly, AC stacking could be obtained by shifting the upper SiS layer of AA structure by *b*/2 along the *y*-axis, as depicted in **Fig. S1(b)**. Initially, AD configuration is attained by *a*/2 along the *x*-axis, followed by *b*/2 along the *y*-axis, as demonstrated in **Fig. S1(c)**.

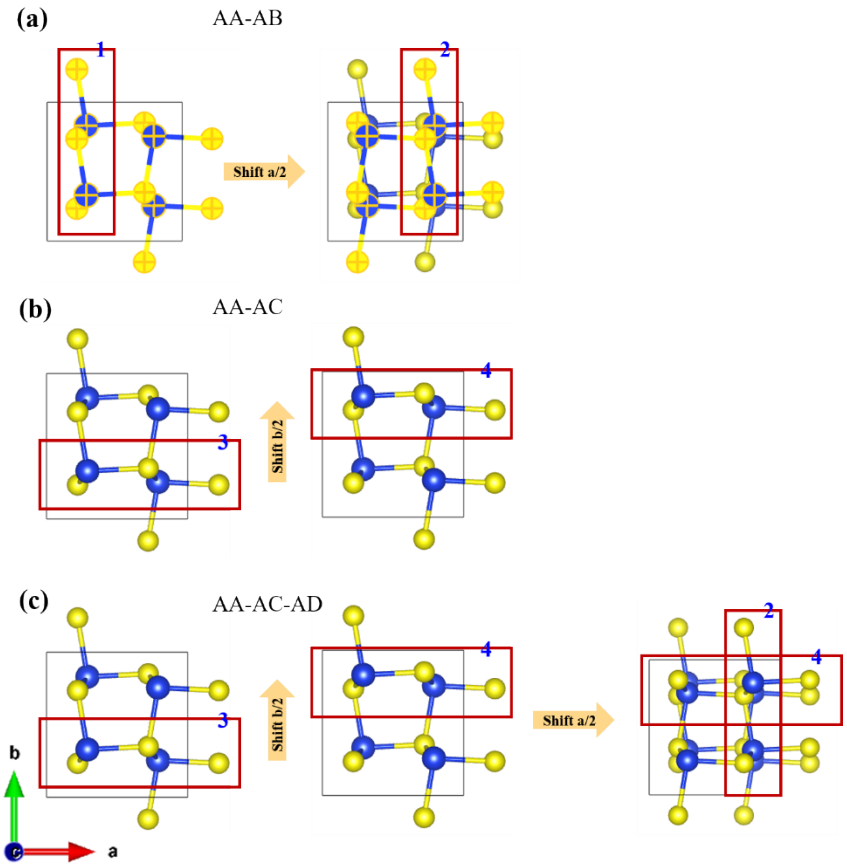

Fig. S1 (a) Interpretation of AA-AB slip path in top views. (b) Interpretation of AA-AC slip path in top views. (c) Interpretation of AA-AD slip path in top views. The emphasized regions (1, 2, 3, 4) are partial sliding changes during the sliding process.

S2. Interpretation of AA, AB and anti-AB stacking in side views.

To clearly identify the difference between AA and AB stacking, we highlighted the region 1 and region 2 to analyze their atomic structure changes. As shown in **Fig. S2(a)** and **(b)**, region 1 shifts *a*/2 along the *x*-axis to reach region 2, inducing a distinct variation in the marked region and then obtaining AB stacking. Furthermore, for AB stacking of bilayer *δ*-SiS, when the polarization of each monolayer is oriented in the same direction, it demonstrates a ferroelectric state, referred to as the AB stacking. Conversely, when the polarization directions of each monolayer oppose each other, it exhibits an antiferroelectric state, termed an anti-AB stacking structure, depicted in **Fig. S2(c)**.

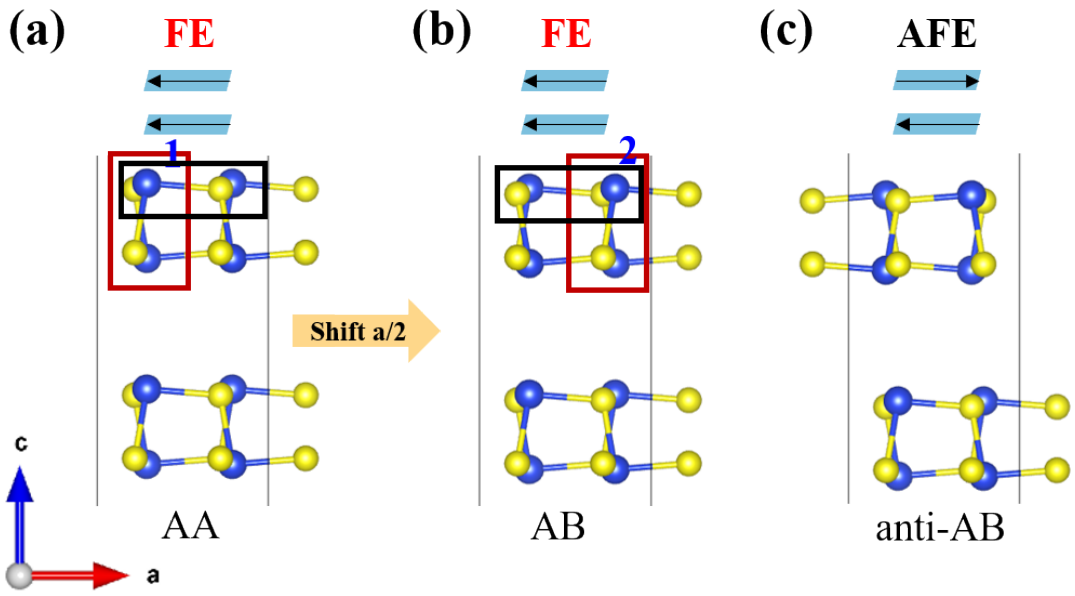

Fig. S2 Side views of (a) AA, (b) AB and (c) anti-AB stacking. The highlighted regions (1, 2) are partial sliding changes during the sliding process. The black rectangular display the difference in AA and AB stacking in the side views.

S3. Available ferroelectric (FE) and anti-ferroelectric (AFE) stackings and their energy difference between FE and AFE state.

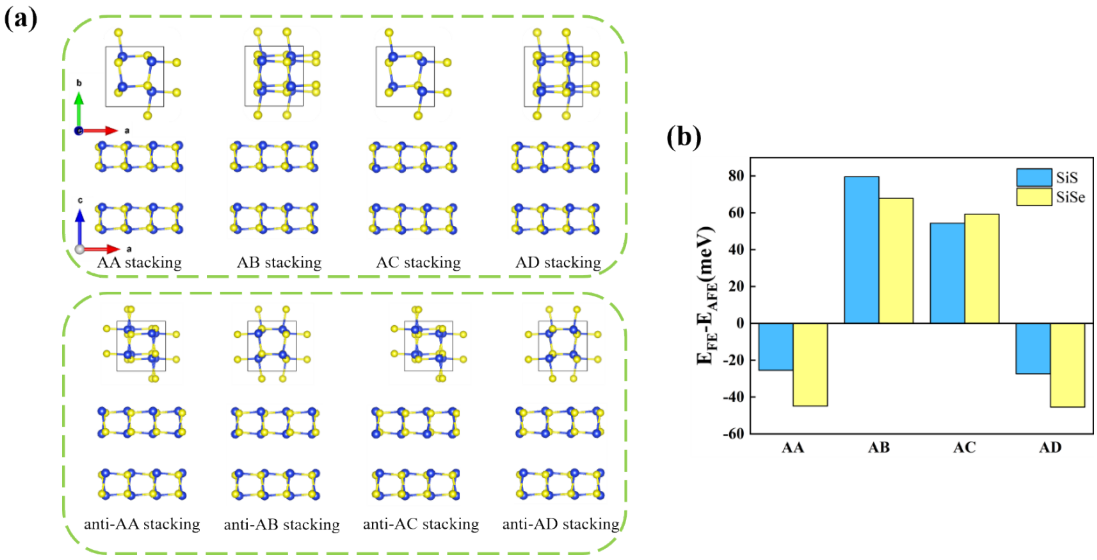

Fig. S3 (a) Top and side views of atomic structures of bilayer δ-SiS (X = S / Se) for FE and AFE state. (b) Total energy difference between FE and AFE state for SiS and SiSe bilayers.

S4. The detailed total energies *E* and energy difference E_{diff} of bilayer δ-SiX (X = S / Se) among all possible stackings.

According to energy computations from Xu *et al.*, E_{diff} can be defined as the energy difference between total energy with different stackings and the lowest energy in FE or AFE state among all stackings.

$$E_{diff} = E - E_{lowest}$$

where E is corresponding energy for different stackings and E_{lowest} is the lowest energy among all stackings in two states (FE and AFE).

By computing the total energies and comparing them systematically in different stackings, we can conclude that bilayer δ-SiX (X = S / Se) prefers to be in AFE state under AB and AC stacking, while being in FE state under AA and AD stacking, listed in **Table S1**. Meanwhile, the lowest energy in bilayer SiS or SiSe is set as a reference to reflect the energy difference among different stackings and states intuitively.

Table S1 The total energies E and energy differences E_{diff} for per unit of AA, AB, AC and AD stacking of bilayer δ-SiX (X = S/Se) under FE and AFE state. The emphasized data are the lowest energy among eight stackings, considering FE and AFE states.

Materials	Stackings	FE state		AFE state	
		E (eV)	E_{diff} (meV)	E (eV)	E_{diff} (meV)
SiS	AA	-78.814	211	-78.788	237
	AB	-78.946	79	**-79.025**	**0**
	AC	-78.785	240	-78.839	186
	AD	-78.769	256	-78.742	283
SiSe	AA	-73.113	868	-73.068	913
	AB	-72.995	986	-73.063	918
	AC	-72.922	1059	**-73.981**	**0**
	AD	-73.067	914	-73.022	959

S5. Atomic structures of reversible AFE-FE-AFE transition through mechanical interlayer sliding along the path AC_{AFE}-AD_{FE}-AC_{AFE} of bilayer δ-SiS.

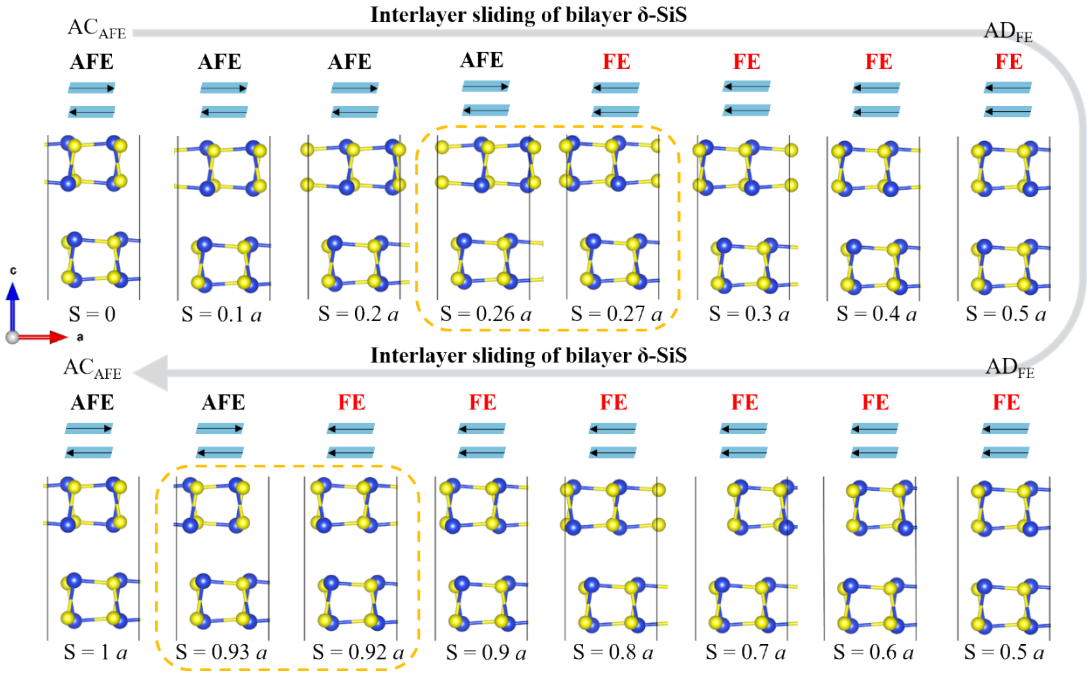

Fig. S4 Atomic structures of reversible AFE-FE-AFE transition under mechanical interlayer sliding for bilayer δ-SiS of AC stacking. Parameter a is the lattice constant in the x-direction.

S6. Atomic structures of reversible AFE-FE-AFE transition through mechanical interlayer sliding along the path AC_{AFE}-AD_{FE}-AC_{AFE} of bilayer *δ*-SiSe.

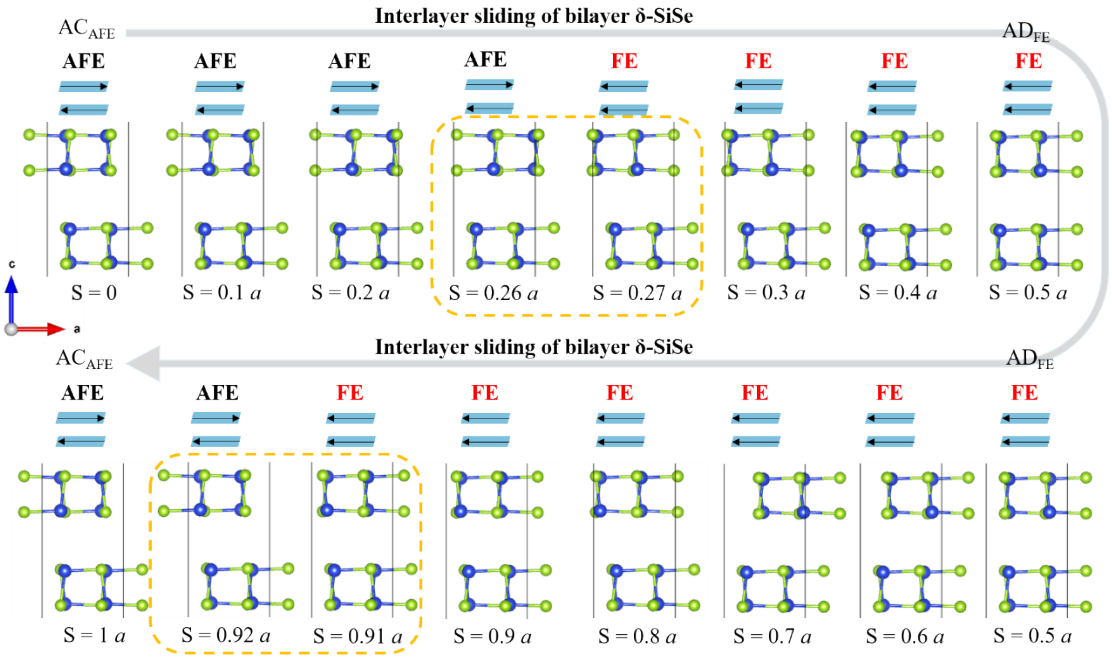

Fig. S5 Atomic structures of reversible AFE-FE-AFE transition under mechanical interlayer sliding for AC stacking of bilayer *δ*-SiSe. Parameter *a* is the lattice constant in the *x*-direction.

S7. Variations in relative energy and polarization under the path AC_{AFE}-AD_{FE}-AC_{AFE} for bilayer *δ*-SiSe.

As shown in **Fig. S6(a)**, for AC_{AFE}-AD_{FE}-AC_{AFE} transition, total energy of bilayer SiSe in the AC_{AFE} stacking initially decreases to 0 at a sliding distance of 0.2 *a*, gradually rises to realize the AFE-FE transition between 0.26 *a* and 0.27 *a*, steadily increases up to 5.88 meV/atom at the AD_{FE} stacking, and finally exhibits a large increasement of 10.06 meV/atoms to its utmost until it reaches original position. Also, the polarization magnitude reaches up to ~70 μC/cm^2 with the sliding distance increasing, also indicates a reversible AFE-FE-AFE transition during the AC_{AFE}-AD_{FE}-AC_{AFE} sliding process, shown in **Fig. S6(b)**.

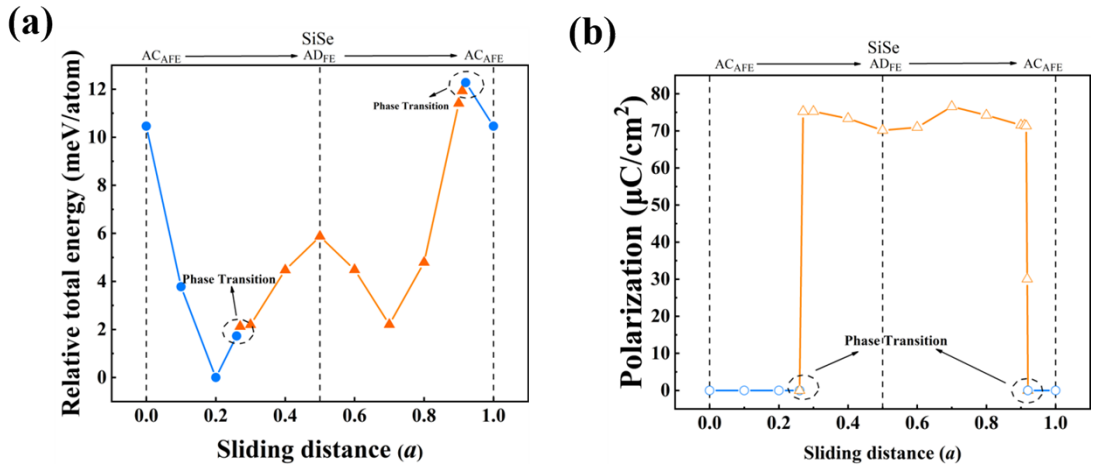

Fig. S6 Variations in relative energy and polarization under the path AC_{AFE}-AD_{FE}-AC_{AFE}. (a) The relative total energy and (b) polarization curve of bilayer *δ*-SiSe.

S8. Phonon spectrum of bilayer δ-SiS in AA_{FE} stacking.

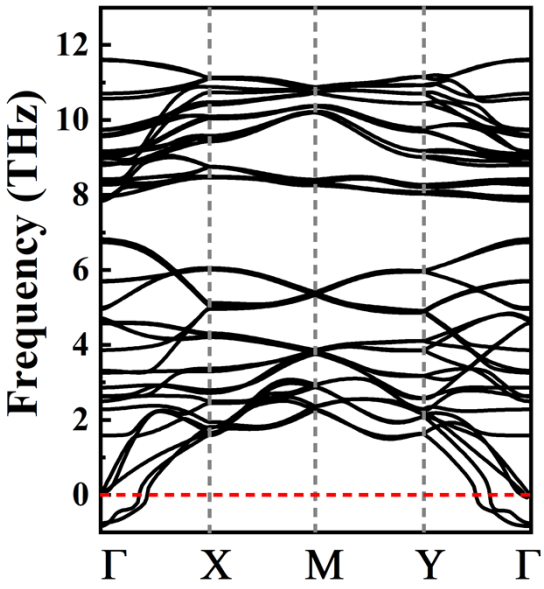

Fig. S7 Phonon spectrum of bilayer δ-SiS in AA_{FE} stacking.

S9. Planar average charge density of path AB_{AFE}-AA_{FE}-AB_{AFE} and path AC_{AFE}-AD_{FE}-AC_{AFE} with sliding distance between 0.2 *a* and 0.3 *a*.

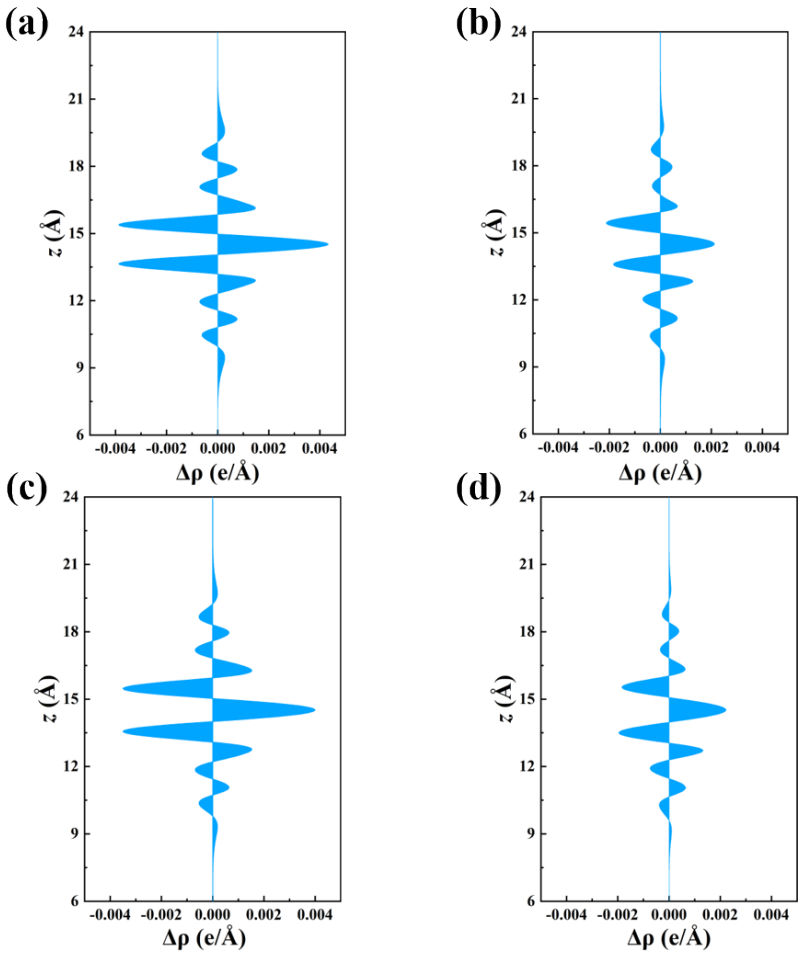

Fig. S8 The planar average charge density of path AB_{AFE}-AA_{FE}-AB_{AFE} with sliding distance between (a) 0.2 *a* and (b) 0.3 *a* and path AC_{AFE}-AD_{FE}-AC_{AFE} with sliding distance between (c) 0.2 *a* and (b) 0.3 *a* for bilayer *δ*-SiS.

S10. Interlayer sliding effect on related lattice parameters and energy for path AC_{AFE}-AD_{FE}-AC_{AFE}.

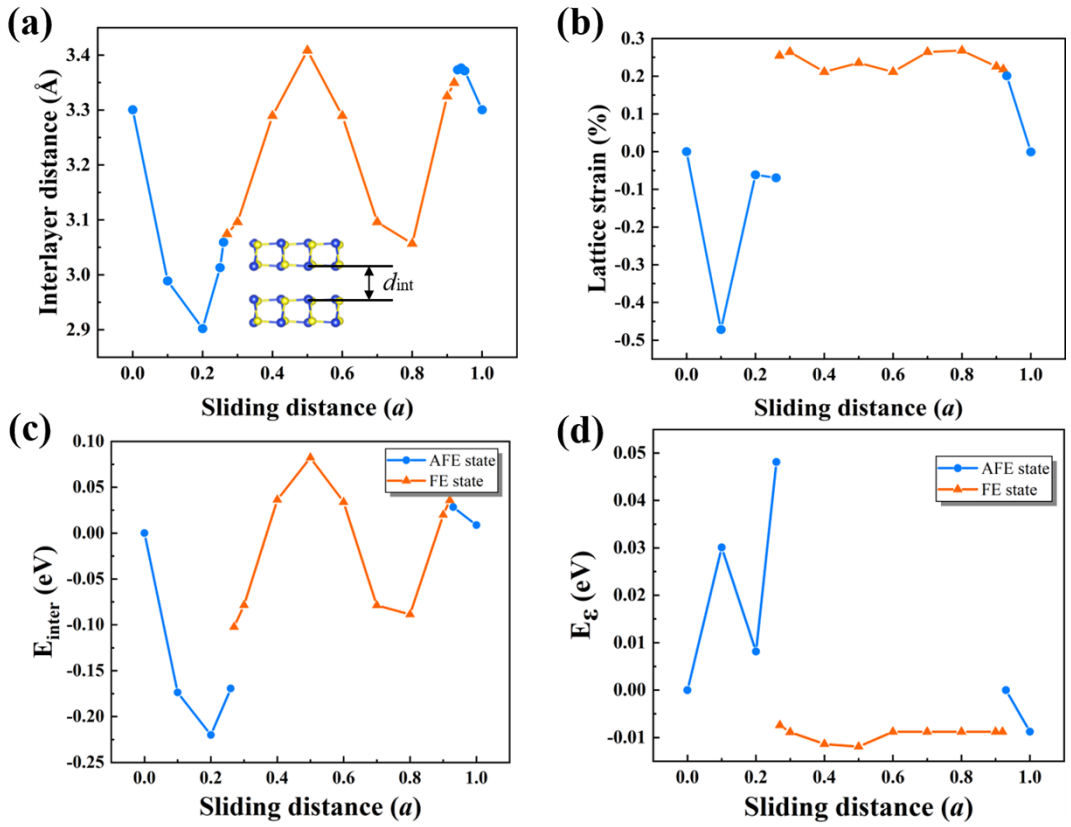

Fig. S9 (a) Interlayer distance change with respect to sliding distance. (b) Lattice strain variation under interlayer sliding moving from 0 *a* to 1 *a*. (c) E_{inter} and (d) E_ε of the relaxed bilayer *δ*-SiS through mechanical sliding.

S11. Interlayer sliding effect on related lattice parameters and energy for path AC_{AFE}-AD_{FE}-AC_{AFE}.

Table S2. Total energies (eV) variations in the sliding process with interlayer distance constrained under AFE and FE state for δ-SiS bilayer.

State	0	0.1	0.2	0.3	0.4	0.5	0.6	0.7	0.8	0.9	1
AB	-78.662	-78.662	-78.661	-78.656	-78.649	-78.645	-78.649	-78.656	-48.661	-78.662	-78.662
anti-AB	-78.667	-78.673	-78.671	-78.659	-78.645	-78.64	-78.644	-78.65	-78.654	-78.659	-78.667

REFERENCES

[1] Bo Xu, Junkai Deng, Xiangdong Ding, Jun Sun, and Jefferson Zhe Liu, npj Computational Materials **8**, 47 (2022).